Electron paramagnetic resonance of sulfur at a split-vacancy site in diamond

J. M. Baker
Oxford Physics, Clarendon Laboratory, Parks Road, Oxford OX1 3PU, United Kingdom

J. A. van Wyk
Department of Physics, University of the Witwatersrand, Johannesburg 2050, South Africa

J. P. Goss* and P. R. Briddon
School of Natural Sciences, University of Newcastle upon Tyne, Newcastle upon Tyne NE1 7RU, United Kingdom

(Received 21 September 2007; revised manuscript received 28 May 2008; published 12 December 2008)

In natural diamonds a sulfur-related paramagnetic center labeled W31 has been previously tentatively assigned to an interstitial sulfur species in a positive charge state. However, we show by combining an assessment of available experimental data and density-functional simulations that the hyperfine tensors can be attributed to a defect made up from sulfur at the center of a divacancy, the so-called split vacancy, in the negative charge state. These acceptors are highly likely to be formed in S-implanted material and are a likely cause for high resistivity in material implanted with sulfur in the attempt to produce *n*-type conduction.

DOI: 10.1103/PhysRevB.78.235203 PACS number(s): 61.72.Bb, 61.72.up, 71.20.Mq

I. INTRODUCTION

The application of diamond to electronics has been hindered by the lack of shallow donors. Sulfur is a candidate and, with two additional valence electrons relative to carbon, is potentially a double donor. This is the case for sulfur in silicon; but the donor level is relatively deep at 0.29 eV,[1] whereas for phosphorus it is just 44 meV.[2]

In diamond, sulfur may be incorporated during growth, and devices have been demonstrated.[3–7] However, the specific role of sulfur is not clear. For example, early reports[8,9] on shallow sulfur donors are most likely related to *p*-type conduction from the accidental boron contamination.[10] Sulfur plays a role in the gas-phase chemistry[11–14] and it is incorporated during growth.[6,15,16]

Donor levels from such sulfur doping are reported from 0.38 to 0.75 eV.[8,9,17] Implantation-related donor levels are reported in the 0.19–0.42 eV range.[4,18,19] However, the origin of the donor levels is unclear. The simplest candidate is substitutional sulfur (S_s). While some calculations support this model,[20–22] the majority suggests a deep donor level lying 0.77 eV or deeper.[23–33] The deep level is attributable to the localization of the donor electron with the S atom moving off site.[26,28,30,31]

Recent interpretation of the available data is suggestive of a combined role for S with boron and/or hydrogen in the donor activity of sulfur-containing material,[33] and that the doping from implantation is either wholly[34] or partly damage related.[18] The interaction of sulfur with other defects and in particular lattice vacancies may be important in conduction and compensation.[34,35]

It is therefore important to identify such defects involving sulfur directly. A potent chemically sensitive probe is electron-paramagnetic-resonance (EPR) spectroscopy. In particular, the $S=1/2$ W31 EPR center has been identified as arising from sulfur.[36] The chemical identification is made from analysis of the relative intensity of the hyperfine lines corresponding to the 0.7% natural abundance of ^{33}S. It was suggested that W31 might arise from a positively charged interstitial sulfur center (S_i^+).

Since the initial report and analysis[36] of W31, the general understanding of preferred sites for large impurity species has improved with clear experimental assignments of examples of complexes involving a lattice vacancy: Si, Ni, and Co.[37–39] In the light of these more recent identifications, the model of an interstitial sulfur species may perhaps be viewed with some skepticism. Therefore, in this study, details of the W31 EPR data are reviewed and an assessment of their interpretation is given in Sec. II. Since an unambiguous identification of sulfur center would be of significance to the development of sulfur-based *n*-type doping, we present in Sec. III the results of density-functional simulations of sulfur-containing defects in diamond and show that the simulations support the conclusions drawn from the re-evaluation of the experimental data for the W31 EPR center.

II. RE-EVALUATION OF EXPERIMENTAL DATA

Since the previous interpretation of the experimental data in terms of S_i^+ is somewhat ambiguous, it is valuable to review the original data. So far as we are aware, W31 has not been reported since the original work and the results of that work are difficult to check at this distance of time; so, apart from limited records of the original measurement, the published evidence of the only reported data[36] is what re-evaluation has to be based on.

The EPR is described in terms of a spin Hamiltonian

$$H = S \cdot g \cdot B + S \cdot A \cdot I + \sum_i S \cdot A^i \cdot I^i,$$

where A is the hyperfine tensor for ^{33}S ($I=3/2$) and A^i are hyperfine tensors for ^{13}C neighbors ($I=1/2$).

The W31 defect has trigonal symmetry about ⟨111⟩ with $g_\parallel=2.0020$ and $g_\perp=2.0025$. The reported[36] hyperfine parameters of the spin Hamiltonian are listed in Table I, including the parameters for three distinct shells of ^{13}C equivalent

TABLE I. Measured hyperfine tensors (MHz), the direction of $A_{\|}$ in terms of the cubic axes (θ,ϕ), and numbers of equivalent neighbors (n) in each shell for the W31 EPR center in diamond (Ref. 36).

Site	n	$\lvert A_{\|}\rvert$	$\lvert A_{\perp}\rvert$	$A_{\|}(\theta,\phi)$
^{33}S	1	1029	1034	54.7, 45
^{13}C[a]	4	70.6	45.1	61, −135
^{13}C[b]	6	14.9	9.8	⟨111⟩ [a]
^{13}C[c]	12	4.8	4.8	Isotropic

[a]It is not stated which ⟨111⟩ direction.

neighbors. Also given is the number (n) of equivalent neighbors in each shell, as judged from the intensity of the ^{13}C satellites relative to the ^{33}S hyperfine lines.

As the authors of Ref. 36 recognized, there are some inconsistencies in the data, so it is necessary to consider it in detail. There are two issues to consider: (a) how sure is the identification of the impurity atom involved in W31 as sulfur and (b) how sure is the attribution to the interstitial site.

The identification of sulfur is based on the ratio of the sum of the intensities of the four hyperfine lines, $I=3/2$, shown in Fig. 1 of Ref. 36 to that of the "central" line measured as 0.7%. It is noted that ^{33}S ($I=3/2$ with 0.74% natural abundance) is the only isotope of sulfur with $I>0$. Figure 2 of Ref. 36 shows sufficient signal/noise ratio to indicate that any other isotope of the impurity with $I>0$ must have at least an order of magnitude lower natural abundance. Estimation of the intensity of the central line due to isotopes with $I=0$ is made difficult by its overlap with lines of several other defects [P1,[40] OK1,[41] and N3 (Ref. 42)] and has to be judged from the changes in intensity produced by annealing and bleaching. This indicates that 0.7% must be fairly close to the natural abundance, which rules out many possible elements with high abundance of isotopes with $I=3/2$. The only serious possible alternative to sulfur appears to be nickel (^{61}Ni is 1.13% abundant). However, the defects caused by the incorporation of nickel in diamond are well known: W8 (Ni_s^-) (Ref. 43) and NE1–3 (Ni at various split-vacancy sites with some nearest-neighboring nitrogen atoms).[37] Hence, there seems little doubt that the attribution of W31 to sulfur is correct.

The attribution of the interstitial site is more problematic. Around the site of an impurity in diamond, such as sulfur, the neighboring carbon atoms are grouped in shells, equidistant (at least in the undistorted lattice) from the site of the impurity, and those which are related to one another by the symmetry operations of the site are described as *equivalent neighbors*.

Both the substitutional and the interstitial sites for an impurity like S have T_d symmetry. For a paramagnetic impurity, the symmetry of the Zeeman tensor (g) and the hyperfine tensor A of ^{33}S would reflect this symmetry. The numbers in the first three shells of equivalent carbon neighbors in each of these defects are given in Table II. The T_d site symmetry of a neighbor is lowered by the presence of the impurity, and its ^{13}C A^i tensor would reflect this lowered symmetry. The A^i tensors of equivalent neighbors are the same except for the rotations appropriate to the symmetry operations of the site.

TABLE II. Numbers of carbon neighbors of a sulfur impurity in various shells appropriate to tetrahedral sites and in various sets appropriate to trigonal models discussed in the text. The symmetry of the neighbor sites for the first shell is indicated.

Model	Symmetry	Nearest	Next nearest	Third shell
S_s	T_d	4 ⟨111⟩ C_{3v}	12 ⟨110⟩	12 ⟨113⟩
S_i	T_d	4 ⟨111⟩ C_{3v}	6 ⟨110⟩	12 ⟨113⟩
S_s	C_{3v}	1 C_{3v}, 3 C_{1h}	3, 3, 6	3, 3, 6
S_i	C_{3v}	1 C_{3v}, 3 C_{1h}	3, 3	3, 3, 6
S_s-V	C_{3v}	3[a] C_{1h}	3[a]	
VSV	D_{3d}	6 $\langle 33\bar{1}\rangle$ C_{1h}	12 $\langle 51\bar{3}\rangle$	6 ⟨155⟩

[a]See text.

The interstitial site was suggested for W31 by Ref. 36 because the values of n for the three shells listed in Table I are the same as those for the T_d site of S_i listed in Table II. However, if the site symmetry of the impurity defect is lowered to trigonal, each of these shells is broken up into smaller sets, with those in each set being related by the threefold rotation about the trigonal axis of the defect, and it is the neighbors in these sets which may be regarded as equivalent neighbors. These are also listed in Table II. How much difference is there between the sets for any shell depends on the magnitude and nature of the symmetry-lowering mechanism. The largest amount of evidence, and the easiest to measure, is that for the first shell, so we shall concentrate on that.

There is another consequence of the reduction in the symmetry of the site. In diamond there are four differently orientated sites of an impurity-containing defect with trigonal symmetry, which are *equivalent sites* related by the symmetry operations of the diamond structure (inversion is not detected by EPR). In each site, there are four neighbors in the first shell, so over all of the sites we need to consider 16 neighbors. As the natural abundance of ^{13}C is 1.1%, there is a 1.1% probability that each of these neighbors might be ^{13}C, with $I=1/2$, which is the only isotope of carbon with nonzero nuclear spin. The hyperfine interaction for ^{13}C at each of the neighboring sites is described by an A^i tensor, which has C_{3v} symmetry for neighbors on the trigonal axis of the defect and C_{1h} symmetry with a {110} plane of reflection symmetry for off-axis neighbors, which are equivalent neighbors as they are related to one another by threefold rotation about the trigonal axis of the defect. Each of the n neighbors in a shell will give rise to a pair of ^{13}C hyperfine lines of 0.5% the intensity of, and equally spaced about, the central line due to even isotopes. As the probability of there being two or more ^{13}C nuclei in a shell is negligible, the total hyperfine structure of the defect comprises n pairs of such lines. So, in a spectrum for four equivalent defect sites there will be $4n$ hyperfine lines on each side of the four central lines due to sites without ^{13}C neighbors. For a general direction of $\vec{B}$ these lines may be resolved, but for high-symmetry directions or in high-symmetry planes many of them are superimposed. The total number n of atoms in the shell may be deduced from the sum of their intensities relative to the cen-

TABLE III. The (number observable) and the relative intensities of separate ^{13}C hyperfine lines on each side of the spectrum centered on $B(\alpha)$ expected for neighbors in the first shell for high-symmetry directions in the crystal. The value of α appropriate to each line is given in square brackets. Experimental values are taken from Fig. 3 of Ref. 36.

Model	⟨100⟩	⟨111⟩	⟨110⟩
S_s or S_i (T_d)	(1) 16 [55]	(2) 1, 3 [0] (2) 3, 9 [70]	(2) 4, 4 [35] (2) 4, 4 [90]
S_s or S_i (C_{3v})	(3) 4, 4, 8 [55]	(2) 3, 1 [0] (3) 6, 3, 3 [70]	(3) 2, 2, 4 [35] (3) 2, 4, 2 [90]
S_s-V	(2) 4, 8 [55]	(1) 3 [0] (2) 6, 3 [70]	(2) 4, 2 [35] (2) 4, 2 [90]
VSV	(2) 4, 8 [55]	(1) 3 [0] (2) 6, 3 [70]	(2) 4, 2 [35] (2) 4, 2 [90]
Expt.	(2) 1, 2 [55]	(1) [0] (2) [70]	(2) [35] (2) [90]

tral line. For the measurements on W31, the center of the spectrum is cluttered with lines from other defects, so for greater precision the sum of the intensities of ^{13}C satellites in a shell has been compared with the sum of the intensities of the ^{33}S hyperfine lines.

Figure 3 of Ref. 36 shows the "road map," the angular variation in the EPR spectrum as a function of the direction of the applied magnetic field $\vec{B}$, in a {110} plane. Two factors influence these line positions: the A^i tensor, which determines the separation of the pair of lines from each neighbor and the g tensor, which determines their mean position, which is the same as the position of the central line at magnetic field $B(\alpha)$ given by $g(\alpha)\mu_B B(\alpha)=h\nu$, where α is the angle between $\vec{B}$ and the trigonal axis of the defect. $g(\alpha)$ is given by $g(\alpha)^2=g_\parallel^2 \cos^2\alpha+g_\perp^2 \sin^2\alpha$.

Table III lists the number of superimposed lines, and hence their relative intensities, one would expect in the groups of hyperfine lines along the high crystal symmetry directions ⟨100⟩, ⟨111⟩, and ⟨110⟩ together with the value of α for that group. Both Fig. 2 of Ref. 36, showing the spectrum for ⟨100⟩, and Fig. 3 of Ref. 36, showing the road map for the group with the largest hyperfine splitting, show clearly that there are two lines on each side for ⟨100⟩, which is inconsistent with S_s or S_i in a C_{3v} site. It would be possible to reduce the number of lines to the observed two by accidental coincidences, leading to ratios of intensities of 1:1 or 3:1. The ratio of intensities of these two lines in Fig. 2 of Ref. 36 is clearly 2:1 and not 1:1 or 3:1. One cannot divide two lines of intensity ratio 2:1 between four neighbors, so the spectrum of Fig. 2 of Ref. 36 indicates that n is a multiple of 3. Furthermore, the road map {110} shown in Fig. 3 of Ref. 36, is consistent with $n=3$, both in the separation of the lines and in their mean positions. Figure 1 shows a reconstruction of the road map using the parameters of Ref. 36 for comparison with Fig. 3 of Ref. 36.

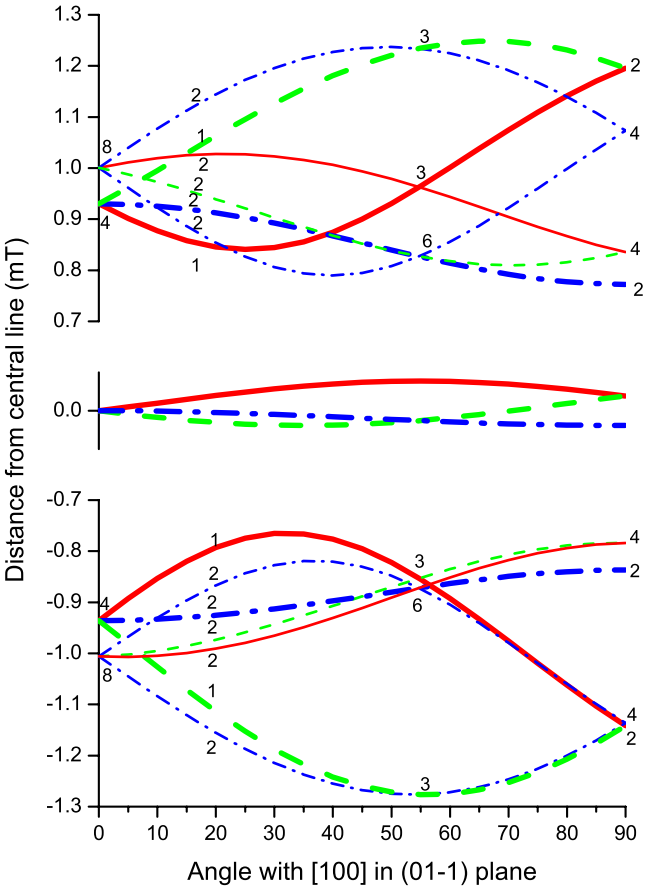

FIG. 1. (Color online) Road map (angular variation of spectral line positions) for $(01\bar{1})$ from [100] through [111] to [011]. All four C_{3v} sites (threefold axes along [111], $[1\bar{1}\bar{1}]$, $[\bar{1}\bar{1}1]$, and $[\bar{1}1\bar{1}]$: EPR is not sensitive to inversion) have three off-axis neighbors with C_{1h} symmetry relative to a {110} plane. One of these symmetry planes for each C_{3v} site contains [100]. Their road maps correspond to the thick lines. The others are shown by thin lines. The C_{3v} sites are indicated by (red) continuous lines for [111], (green) dashed lines for $[1\bar{1}\bar{1}]$, and (blue) dot-dash-dot lines for both $[\bar{1}1\bar{1}]$ and $[\bar{1}\bar{1}1]$ which are superimposed. The number of superimposed lines is shown adjacent to the lines and crossing points. The thick (red) continuous, (blue) dot-dash-dot, and (green) dashed lines at the center show the angular variation because of the anisotropy of $B(\alpha)$ for the central lines due to sites without any ^{13}C neighbor. Although this road map was generated using the ^{13}C hyperfine parameters given by Ref. 36 for three off-axis nearest neighbors in C_{3v} sites, the road map would be identical for the six nearest-neighbor sites in VSV (with D_{3d} symmetry) with the same hyperfine parameters, as these neighbors are related in pairs by inversion symmetry in the S atom site.

Note that this reconstruction accounts for all of the observed lines. There is no evidence of an on-axis neighbor, which would have extreme separation for [111], at 55° from [100], equally spaced around a mean $B(0)$ (continuous red line). Even if such a line was hidden beneath one of the extreme solid green and dashed blue lines at this angle, the counterpart of the other side of the spectrum would have been well resolved.

TABLE IV. Calculated hyperfine tensors (MHz) for ^{33}S, with ^{13}C sites identified in Fig. 5, in spherical polar relative to the cubic axes. n indicates the number of equivalent sites for the [111] orientation of S_s^+ and $(VSV)^-$ centers in diamond.

Site	n	$\|A_1\|$	$A_1(\theta,\phi)$		$\|A_2\|$	$A_2(\theta,\phi)$		$\|A_3\|$	$A_3(\theta,\phi)$	
					S_s^+					
S	1	149	54.7	45.0	49	129.0	100.0	49	121.3	−19.6
C_1	1	214	54.7	45.0	167	127.8	101.8	167	122.6	−18.0
C_2	3	62	34.1	−135.0	47	56.0	45.0	45	90.0	−45.0
					$(VSV)^-$					
S	1	1073	119.2	−21.7	1073	49.1	−82.7	1069	54.7	45.0
C_1	6	69	61.4	−135.0	45	90.0	−45.0	44	28.6	45.0
C_2	12	−4	50.7	−39.6	−3	114.9	−107.3	−2	49.6	−173.9
C_3	6	15	50.3	45.0	9	90.0	−45.0	9	140.3	45.0
C_4	6	7	176.2	−135.0	5	93.8	45.0	5	90.0	−45.0

We will consider this in the light of simple models of trigonal symmetry. The properties of those considered are listed in Table II. First consider the simplest models for reducing the T_d symmetry of the S_s and S_i sites to trigonal. For S_i we suppose that the local distortion makes one of the four nearest neighbors (that on the trigonal axis) different from the other three. For S_s a similar distortion can happen by making one of the ligand bonds different from the other three. Also for S_s, one of the neighbors may be missing leaving a S_s-V site, so S_s has only three neighbors in the first shell (but there are three neighbors of the vacancy with dangling bonds which are more important than the neighbors of S). The S atom may also occupy a split-vacancy site, at the center of a divacancy, with D_{3d} symmetry, which we write as VSV, coordinating with six neighbors in its first shell related by inversion symmetry.

For trigonally distorted S_s or S_i, it is possible that the lines due to the on-axis neighbor are not observed because they are obscured by some other part of the spectrum, such as the ^{14}N hyperfine lines of P1,[40] whose intensity is about seven times that of any missing lines. The hyperfine A matrix for these would need to be nearly exactly twice that of ^{14}N in P1, i.e., $A_\parallel \sim 228$ MHz and $A_\perp \sim 163$ MHz. In principle such lines could have been observed unobscured on either side of the ^{33}S hyperfine lines at the same intensity as those shown in the lower trace of Fig. 2 of Ref. 36 at ± 1 mT, i.e., with a signal/noise ratio of 2 or 3. Unfortunately it is not clear whether this part of the spectrum was examined carefully. Supposing that these were the explanation of missing lines, it is difficult to understand how A for an on-axis neighbor of S_i could be so different in magnitude from the off-axis neighbors, so S_i is an unlikely model. It would be possible for S_s, but comparison with the analogous case of P1, N_s^0, suggests that one would expect the A matrix for ^{33}S to be much more anisotropic (see also Table IV), and one would expect a large spin density on other sets of three ^{13}C hyperfine lines for other shells.[42] The road map is consistent with the $(S_s\text{-}V)^0$ model, the analog of $(N_s\text{-}V)^-$ W15,[44] but only 28% of the spin density is located on the three carbon neighbors in W31 compared with ~95% on the three neighbors of the vacancy in $(N_s\text{-}V)^-$.

That leaves the $(VSV)^-$ model, for which $n=6$, but as the carbon ligands are related by inversion symmetry, the road map would be like Fig. 1. This model is consistent with every aspect of the observed spectrum except for the value of $n=4$ given by Ref. 36 for the first shell. Measurement of relative intensities of lines has become common place with modern integration and line reconstruction techniques, but it was more problematic in the days of pen recorders. The relative intensities of the ^{13}C and ^{33}S lines were judged using the amplitudes of derivative line shapes, so it would be sensitive to differences in line width. Misalignment, or mosaic spread, would probably contribute more to the width of ^{13}C lines because of their greater anisotropy, which would reduce the apparent value of n for the first shell. A reassessment of such records of the original data that remain suggest that the published value of $n=4$ for the first shell is an underestimate rather than an overestimate.

Hence, overall, the experimental evidence, although not unambiguous, tends to favor the $(VSV)^-$ model. We now present the results of density-functional simulations to assess further the various sites for sulfur in relation to the W31 center.

III. COMPUTATIONAL ANALYSIS

A. Method

Calculations were carried out using the spin-density-functional technique implemented in *ab initio* modeling program (AIMPRO) (Refs. 45 and 46), both with local-density[47] and generalized-gradient[48] approximations (denoted as LDA and GGA, respectively). The wave-function basis consists of atom-centered Gaussians.[49] Carbon atoms are treated using linear combinations of s and p orbitals with the addition of d functions to allow for polarization. Sulfur impurities are treated using independent sets of s and p Gaussians with four widths, respectively, with the addition of three sets of d-polarization functions. The charge density is Fourier transformed using plane waves with a cutoff of 350 Ry, yielding well-converged total energies. Core electrons are eliminated

by using norm-conserving pseudopotentials.[50]

Using the above procedure with the LDA functional, the lattice constant and bulk modulus of bulk diamond are reproduced to within ~1% (an underestimate) and 5%, respectively, of experiment. For the GGA, the agreement is similar at around 1 and 2%, with the lattice constant slightly overestimated in this case. The calculated direct and indirect band gaps are close to previously published plane-wave values.[51]

To model the defects, 216-atom cubic supercells of side length $3a_0$ have been used. The Brillouin zone is sampled using the Monkhorst-Pack scheme.[52] Hyperfine interactions are modeled as outlined previously.[53] Briefly, this involves the combination of pseudopotentials and reconstructed all-electron wave functions in the core region.[54,55] Reconstruction of the ion cores allows us to calculate the hyperfine tensor elements within a frozen-core all-electron wavefunction approximation, without the computational difficulties associated with a full all-electron calculation.

The zero-temperature formation energy of a system X in charge state q may be calculated using

$$E^f(X,q) = E(X,q) - \sum \mu_i + q(E_v^X + \mu_e). \quad (1)$$

Here E is the total energy, μ_i and μ_e are the chemical potentials of the atoms and electrons, respectively, and E_v^X is the energy of the valence-band top. Donor or acceptor electrical levels may be estimated using the formation energy method or by the use of the marker method.[49] Binding energies E^b are defined as positive if the reaction $A+B \rightarrow AB$ is exothermic.

Finally, reaction energies are obtained using the climbing nudged-elastic-band (NEB) method.[56,57]

We modeled substitutional and interstitial sulfur (S_s and S_i) and the split-vacancy-sulfur complex (VSV). For each system we have investigated the geometry, electronic structure, electrical activity, and (for paramagnetic systems) the hyperfine interactions. We present the results for each of these in turn.

B. Structure and energetics

S_s in the neutral and positive charge states moves from the substitutional site, and in the positively charged paramagnetic form, possesses trigonal C_{3v} symmetry, as shown in Fig. 2(a). In the LDA (GGA) calculations, the unique C–S dilated "bond" is 17% (16%) longer than a host C–C bond, with the three equal C–S bonds also dilated, but by the smaller amount of 9% (10%). The barrier to reorientation is small. The LDA and GGA calculations yield 70 and 90 meV, respectively. We conclude that S_s^+ might reorient relatively freely even at low temperatures. We return to this in Sec. III D.

Interstitial impurities take several forms. One is an atom or ion residing in the cages within the lattice, such as interstitial alkali metals.[58,59] Alternatively, the interstitial may combine with the lattice, such as the self-interstitial (I) (Refs. 60–62) and interstitial nitrogen,[63] or even be unstable and displace a host atom forming a substitutional impurity and a self-interstitial, such as predicted for interstitial silicon.[64]

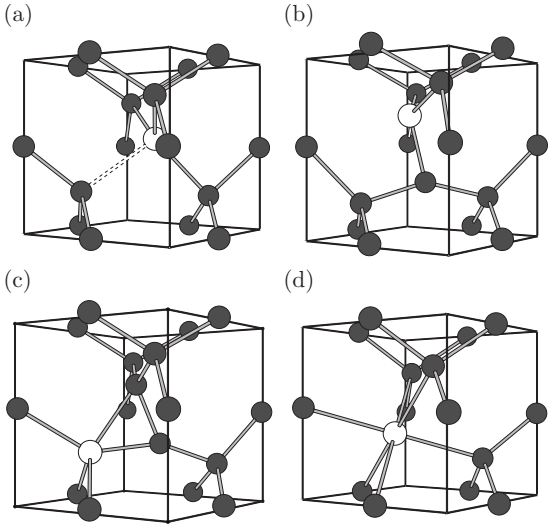

FIG. 2. Schematic structures of (a) S_s^+, (b) S_i, (c) S_s-I, and (d) VSV. Dark and light atoms are C and S, respectively, and the cubes indicate the underlying cubic lattice of diamond.

We analyzed many starting configurations including the nonbonded, bond-centered, split interstitials, and randomized structures. The lowest energy form is a [001]-oriented split interstitial where the S atom is slightly displaced from the [001] axis, shown in Fig. 2(b). There is *no barrier* to the reaction of a cage-sited interstitial sulfur with the lattice to produce this structure, and constrained T and H sites are 12 and 7 eV higher in energy, respectively. We therefore discount the nonbonded interstitial structures.

The form in Fig. 2(b) is only metastable, and the energy is lowered by 2.2 eV by exchange with a carbon neighbor producing a S_s-I complex shown in Fig. 2(c). There is a 2.5 eV barrier to interconversion between S_i and S_s-I, as obtained using the NEB method with 19 images. Thus, S_i shown in Fig. 2(b) is unlikely to be present both on the basis of formation energy and thermal stability, and we may discount this structure too.

Finally, as previously discussed[35] a VSV complex is trigonal, transforming under the D_{3d} point group, and in the *negative* charge state possesses a single unpaired electron.[65] As noted above, the complex of a lattice vacancy and a sulfur atom, in common with many other impurities,[35] is of the split-vacancy form, with an interstitial sulfur impurity lying at the center of a divacancy. The structure is shown in Fig. 2(d) is in contrast with structures comprised from a lattice vacancy neighboring a substitutional impurity, such as the structure adopted by nitrogen. The split-vacancy configuration is found to be adopted by impurities with covalent radii substantially greater than the host carbon atoms,[35] and there is also some evidence linking the split-vacancy model to experimental centers for silicon-vacancy centers,[39,64,66] as well as Ni- and Co-vacancy complexes, some also involving nitrogen.[37,38]

The relative stability of the configurations in Fig. 2 is obtained from their formation energies. We find $E^f(S_i) - E^f(S_s) = 8.9$ eV, $E^f(S_s\text{-}I) - E^f(S_s) = 6.8$ eV, and $E^f(S_s) - E^f(VSV) = 4.3$ eV using the LDA. The corresponding GGA values are 8.7, 6.7, and 4.2 eV, indicating independence from

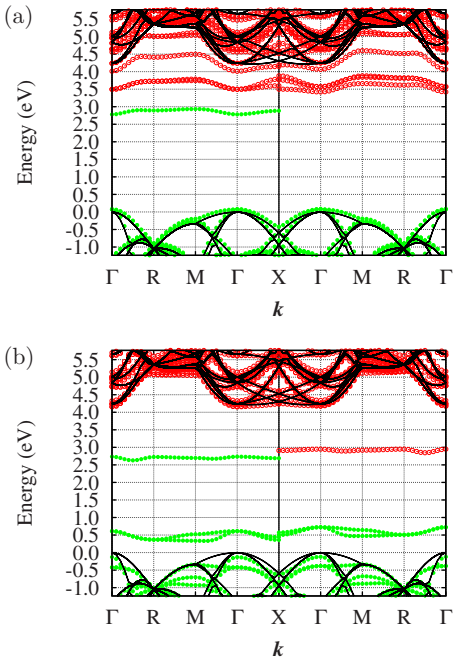

FIG. 3. (Color online) Kohn-Sham bands in the vicinity of the band gap along high-symmetry directions of the first Brillouin zone of a 216-atom supercell containing (a) S_s^+ and (b) $(VSV)^-$. Filled (green) filled circles show occupied levels and empty (red) circles show empty bands. Black lines are defect-free bands. The zero of energy is defined as the valence-band top of diamond.

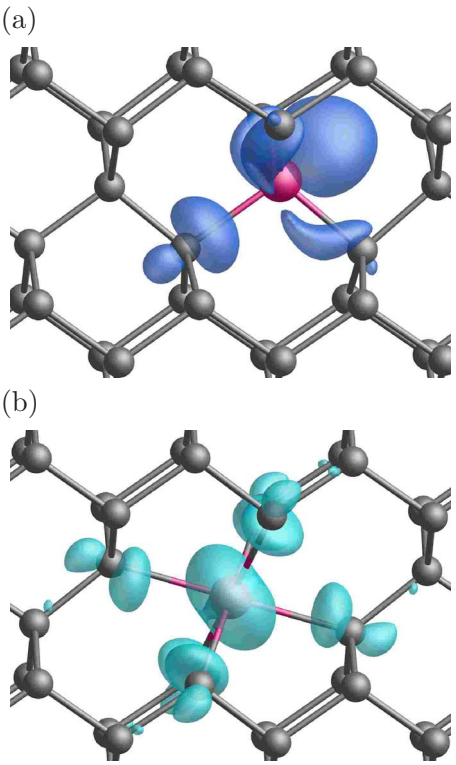

FIG. 4. (Color online) Electron density for the unpaired electrons in (a) S_s^+ and (b) $(VSV)^-$. Dark and light atoms are C and S respectively.

the choice of functional. The formation energies show in order of increasing thermodynamic stability; we have $S_i \rightarrow S_s$-$I \rightarrow S_s \rightarrow VSV$.

In the cases of S_s-I and VSV, it is also useful to know the binding energies. S_s-I is bound by 4.8 eV with respect to dissociation into S_s and I. This contrasts to an exothermic reaction for dissociation of a silicon interstitial into a substitutional impurity and I.[64] In the sulfur case, binding is a consequence of in increase in the number of occupied bands high in the band gap during the formation of S_s, which is not the case for silicon. The binding energy of the VSV complex, using $E^f(V)=6.0$ eV,[67] is 10.0 eV.[35,68] Therefore, for long low-temperature anneals, such as experienced by natural S-doped diamond in the geological context or in material implanted with S and annealed at high temperatures, the formation of VSV is highly likely, and subsequent dissociation of VSV is unlikely.

C. Electronic structure

The LDA Kohn-Sham band structure for S_s^+ is plotted in Fig. 3(a). A partially filled band lies toward the top of the band gap, consistent with a deep donor level, and the localization of the unpaired electron is plotted in Fig. 4(a). The spin density is principally comprised of p-polarized contributions, and there is a rather modest proportion localized on the S atom.

The location of the donor level, as indicated in Sec. I, has been the subject of much debate. We find that the donor level of S_s lies 0.2 eV above that of N_s and 0.9 eV below that of P_s, suggestive of a level at $E_c-1.5$ eV.

The band structure of VSV has been presented previously.[35] In Fig. 3(b) we show the band structure of $(VSV)^-$, indicating a midgap level associated with orbitals on the six carbon neighbors and a large contribution from the sulfur atom. The localization is shown in Fig. 4(b). This is in contrast to the $VSiV$ complex responsible for the 12-line optical feature,[66,69] and an $S=1$ EPR signal where the component corresponding to the impurity is rather small.[70]

As suggested by the location of an empty midgap band for $(VSV)^0$,[35] and hinted at in Fig. 3(b), in n-type diamond VSV would thermodynamically adopt the negative charge state. The acceptor level of VSV is calculated by comparison with the calculated electron affinity of the vacancy-nitrogen center which possesses an acceptor level at $E_c-2.583$ eV (Ref. 71). The level is thus found to lie around $E_c-1.6$ eV, which is very close to the donor level of nitrogen[72] and the calculated values for S_s. In particular, for type-Ib material where the W31 EPR center is seen, it is important to assess further whether VSV is negatively charged in thermodynamic equilibrium. Simulations containing both VSV and N_s in the same cell show that $N_s^+ + (VSV)^-$ is lower in energy than $N_s^0 + (VSV)^0$, and we conclude that the acceptor level of VSV lies below the donor level of N_s.

D. Hyperfine Interactions

For both S_s and VSV trigonal systems, Table IV lists the calculated hyperfine tensors for ^{33}S and ^{13}C at the sites indicated in Fig. 5. In contrast to W31, the hyperfine interaction with ^{33}S in S_s^+ is small and the tensor is anisotropic. How-

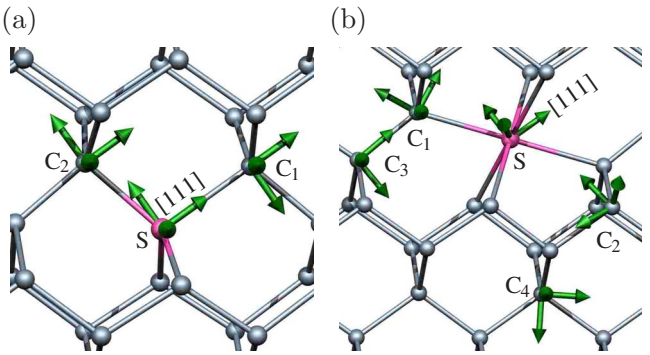

FIG. 5. (Color online) Schematics of (a) S_s^+ and (b) $(VSV)^-$ showing the ^{13}C sites and arrows showing the directions of the hyperfine tensor elements listed in Table IV in each case.

ever, the ^{13}C hyperfine interaction on the unique neighbor is remarkably close to two times that for ^{14}N in P1 (see Sec. II).

In contrast, $(VSV)^-$ yields an isotropic ^{33}S hyperfine interaction in excellent quantitative agreement with W31. $(VSV)^-$ also possesses the correct overall symmetry and is consistent with the revised interpretation of the numbers of equivalent nearest-neighbor ^{13}C sites. In addition:

(1) The magnitudes at the C_1 site (Fig. 5 and Table IV) agree reasonably with C^a (Table I); the angle of the principal component at 29° from [110] also coincides with experiment.[36]

(2) In agreement with the C^b sites, the six C_3 are calculated as approximately axial along [111], and the magnitudes of the hyperfine tensors also agree reasonably.

(3) The C^c sites yield isotropic hyperfine tensors. Both C_2 and C_4 in Fig. 5 are approximately isotropic and of the correct order of magnitude. Since the sign of the C^c hyperfine tensor is undetermined, we cannot distinguish between them and either fit with experiment.

(4) Finally, we note that the magnitude of the C_2 hyperfine interaction is somewhat less than at C_3, despite being closer to the S atom. Indeed, Fig. 4 shows that the polarization of the spin density is directed along ⟨111⟩. Then, in fitting a model to a set of ^{13}C hyperfine interactions, we suggest it can be highly misleading to assume that the magnitudes reflect increasing distance from the core of the EPR center.

The quantitative agreement of the tensor magnitudes and principal directions with the experimental parameters of W31 is excellent. It is therefore tempting to assign W31 to the $(VSV)^-$ system, in confirmation of the tentative assignment of the experimental data in Sec. II, with the critical parameter being the hyperfine tensor for ^{33}S.

For comparison, the hyperfine tensors for ^{33}S and the six nearest-neighbor ^{13}C sites in $(VSV)^-$ calculated using the GGA are very close to those listed in Table IV. In particular, the isotropic component of the A tensor on ^{33}S is 1058 MHz in comparison to 1072 MHz from the LDA. Similarly the principal component of the ^{33}S hyperfine tensor for S_s^+ is 154 MHz using the GGA. Overall we find only small (typically $<5\%$) variations between A tensors using the LDA and GGA functionals, and the choice does not affect the conclusions.

Finally, noting that the reorientation of S_s^+ is easily activated, it seems probable that EPR measurements would average to an isotropic center. Indeed, a low-temperature transition from tetragonal to isotropic is both theoretically[73] and experimentally[74] determined for substitutional phosphorus in diamond, and one might therefore reasonably expect a similar behavior for S_s^+. Combining the hyperfine tensors for the different orientations of S_s^+ yields an isotropic value of 82 MHz on ^{33}S, with $A_{\parallel}^{[111]}$ and $A_{\perp}^{[111]}$ being 88 and 82 MHz on the nearest-neighbor ^{13}C site.

IV. DISCUSSION AND CONCLUDING REMARKS

Of the S_s, S_i, S_s-I, and VSV sulfur centers examined in this study, only S_s and VSV are likely to survive high-temperature annealing. Then, for sulfur incorporated in diamond, S_s^+ and $(VSV)^-$ would be expected to be present subsequent to implantation, where radiation damage is present both to compensate the sulfur donor and lead to the formation of VSV during annealing.

In correlating the W31 EPR center with $(VSV)^-$, it remains to comment on the heat treatment required to produce the EPR center in type-Ib diamond. The location of the electrical levels suggest that both $(VSV)^-$ and N_s^0 centers may be photoionized in the visible range of the spectrum. Then, even if the acceptor level of VSV lies below the donor level of N_s, the recombination process will favor $N_s^+ + e^- \rightarrow N_s^0$ since a larger electron-capture cross section is expected for a positively charged N_s^+ electron trap. This leads to nonequilibrium populations of N_s^0 and $(VSV)^0$, with the latter being diamagnetic. Thermal treatment, however, would tend to drive the system to thermodynamic equilibrium, and since the acceptor level of VSV most probably lies below the donor level of N_s, such heat treatment in the dark would increase the concentration of $(VSV)^-$.

In identifying the W31 center with $(VSV)^-$ we have a direct method for the assessment of the formation of these compensating centers in sulfur-doped material. Furthermore, we have provided a set of predicted hyperfine interactions for S_s^+ that aids direct experimental identification of this center. In this context, it would be of great benefit to produce sulfur-doped material which has an isotopically enriched ^{33}S content.

ACKNOWLEDGMENTS

J.P.G. and P.R.B. gratefully acknowledge the financial support from the EPSRC-GB. We also gratefully acknowledge Solveig Felton for help in preparation of Fig. 1.

*Corresponding author; j.p.goss@ncl.ac.uk

[1] H. Pettersson and H. G. Grimmeiss, Phys. Rev. B **42**, 1381 (1990).
[2] D. Long and J. Myers, Phys. Rev. **115**, 1119 (1959).
[3] H. Okushi, Diamond Relat. Mater. **10**, 281 (2001).
[4] M. Hasegawa, D. Takeuchi, S. Yamanaka, M. Ogura, H. Watanabe, N. Kobayashi, H. Okushi, and K. Kajimura, Jpn. J. Appl. Phys., Part 2 **38**, L1519 (1999).
[5] K. Horiuchi, A. Kawamura, T. Ide, T. Ishikura, K. Takamura, and S. Yamashita, Jpn. J. Appl. Phys., Part 2 **40**, L275 (2001).
[6] E. Trajkov, S. Prawer, J. E. Butler, and S. M. Hearne, J. Appl. Phys. **98**, 023704 (2005).
[7] F. A. M. Koeck and R. J. Nemanich, Diamond Relat. Mater. **14**, 2051 (2005).
[8] I. Sakaguchi, M. N.-Gamo, Y. Kikuchi, E. Yasu, H. Haneda, T. Suzuki, and T. Ando, Phys. Rev. B **60**, R2139 (1999).
[9] M. Nishitani-Gamo, E. Yasu, C. Y. Xiao, Y. Kikuchi, K. Ushizawa, I. Sakaguchi, T. Suzuki, and T. Ando, Diamond Relat. Mater. **9**, 941 (2000).
[10] R. Kalish, A. Reznik, C. Uzan-Saguy, and C. Cytermann, Appl. Phys. Lett. **76**, 757 (2000).
[11] H. Sternschulte, M. Schreck, and B. Stritzker, Diamond Relat. Mater. **11**, 296 (2002).
[12] J. R. Petherbridge, P. W. May, E. J. Crichton, K. N. Rosser, and M. N. R. Ashfold, Phys. Chem. Chem. Phys. **4**, 5199 (2002).
[13] J. R. Petherbridge, P. W. May, G. M. Fuge, G. F. Robertson, K. N. Rosser, and M. N. R. Ashfold, J. Appl. Phys. **91**, 3605 (2002).
[14] J. R. Petherbridge, P. W. May, G. M. Fuge, K. N. Rosser, and M. N. R. Ashfold, Diamond Relat. Mater. **11**, 301 (2002).
[15] S. C. Eaton, A. B. Anderson, J. C. Angus, Y. E. Evstefeeva, and Y. V. Pleskov, Diamond Relat. Mater. **12**, 1627 (2003).
[16] M. Nishitani-Gamo, C. Y. Xiao, Y. F. Zhang, E. Yasu, Y. Kikuchi, I. Sakaguchi, T. Suzuki, Y. Sato, and T. Ando, Thin Solid Films **382**, 113 (2001).
[17] K. Nakazawa, M. Tachiki, H. Kawarada, A. Kawamura, K. Horiuchi, and T. Ishikura, Appl. Phys. Lett. **82**, 2074 (2003).
[18] D. K. Troupis, O. Gaudin, M. D. Whitfield, and R. B. Jackman, Diamond Relat. Mater. **11**, 342 (2002).
[19] J. F. Prins, Diamond Relat. Mater. **10**, 1756 (2001).
[20] A. B. Anderson, E. J. Grantscharova, and J. C. Angus, Phys. Rev. B **54**, 14341 (1996).
[21] H. Zhou, Y. Yokoi, H. Tamura, S. Takami, M. Kubo, A. Miyamoto, M. N.-Gamo, and T. Ando, Jpn. J. Appl. Phys., Part 1 **40**, 2830 (2001).
[22] D. Saada, J. Adler, and R. Kalish, Appl. Phys. Lett. **77**, 878 (2000).
[23] T. Miyazaki and H. Okushi, Diamond Relat. Mater. **10**, 449 (2001).
[24] T. Nishimatsu, H. Katayama-Yoshida, and N. Orita, Physica B **302-303**, 149 (2001).
[25] H. Katayama-Yoshida, T. Nishimatsu, T. Yamamoto, and N. Orita, J. Phys.: Condens. Matter **13**, 8901 (2001).
[26] T. Nishimatsu, H. Katayama-Yoshida, and N. Orita, Jpn. J. Appl. Phys., Part 1 **41**, 1952 (2002).
[27] L. G. Wang and A. Zunger, Phys. Rev. B **66**, 161202(R) (2002).
[28] T. Miyazaki, Phys. Status Solidi A **193**, 395 (2002).
[29] S. J. Sque, R. Jones, J. P. Goss, and P. R. Briddon, Physica B **340-342**, 80 (2003).
[30] S. J. Sque, R. Jones, J. P. Goss, and P. R. Briddon, Phys. Rev. Lett. **92**, 017402 (2004).
[31] E. B. Lombardi, A. Mainwood, and K. Osuch, Phys. Rev. B **70**, 205201 (2004).
[32] J. P. Goss, P. R. Briddon, S. J. Sque, and R. Jones, Diamond Relat. Mater. **13**, 684 (2004).
[33] Y. Cai, T. Zhang, A. B. Anderson, J. C. Angus, L. N. Kostadinov, and T. V. Albu, Diamond Relat. Mater. **15**, 1868 (2006).
[34] E. Baskin, A. Reznik, D. Saada, J. Adler, and R. Kalish, Phys. Rev. B **64**, 224110 (2001).
[35] J. P. Goss, P. R. Briddon, M. J. Rayson, S. J. Sque, and R. Jones, Phys. Rev. B **72**, 035214 (2005).
[36] J. A. van Wyk and J. H. N. Loubser, Mater. Sci. Forum **10-12**, 923 (1986).
[37] V. A. Nadolinny, A. P. Yelisseyev, J. M. Baker, M. E. Newton, D. J. Twitchen, S. C. Lawson, O. P. Yuryeva, and B. N. Feigelson, J. Phys.: Condens. Matter **11**, 7357 (1999).
[38] D. J. Twitchen, J. M. Baker, M. E. Newton, and K. Johnston, Phys. Rev. B **61**, 9 (2000).
[39] A. M. Edmonds, M. E. Newton, P. M. Martineau, D. J. Twitchen, and S. D. Williams, Phys. Rev. B **77**, 245205 (2008).
[40] W. V. Smith, P. P. Sorokin, I. L. Gelles, and G. J. Lasher, Phys. Rev. **115**, 1546 (1959).
[41] P. E. Klingsporn, M. D. Bell, and W. J. Leivo, J. Appl. Phys. **41**, 2977 (1970).
[42] M. Ya. Shcherbakova, E. V. Sobolev, and V. A. Nadolinny, Dokl. Akad. Nauk SSSR **204**, 851 (1972) [Sov. Phys. Dokl. **17**, 513 (1972)].
[43] J. H. N. Loubser and W. P. van Ryneveld, Nature (London) **211**, 517 (1966).
[44] J. H. N. Loubser and J. A. van Wyk, Rep. Prog. Phys. **41**, 1201 (1978).
[45] R. Jones and P. R. Briddon, in *Identification of Defects in Semiconductors*, Semiconductors and Semimetals Vol. 51A, edited by M. Stavola (Academic, Boston, 1998), Chap. 6.
[46] M. J. Rayson and P. R. Briddon, Comput. Phys. Commun. **178**, 128 (2008).
[47] J. P. Perdew and Y. Wang, Phys. Rev. B **45**, 13244 (1992).
[48] J. P. Perdew, K. Burke, and M. Ernzerhof, Phys. Rev. Lett. **77**, 3865 (1996).
[49] J. P. Goss, M. J. Shaw, and P. R. Briddon, in *Theory of Defects in Semiconductors*, Topics in Applied Physics Vol. 104, edited by D. A. Drabold and S. K. Estreicher (Springer, Berlin, 2007), pp. 69–94.
[50] C. Hartwigsen, S. Goedecker, and J. Hutter, Phys. Rev. B **58**, 3641 (1998).
[51] D. A. Liberman, Phys. Rev. B **62**, 6851 (2000).
[52] H. J. Monkhorst and J. D. Pack, Phys. Rev. B **13**, 5188 (1976).
[53] M. J. Shaw, P. R. Briddon, J. P. Goss, M. J. Rayson, A. Kerridge, A. H. Harker, and A. M. Stoneham, Phys. Rev. Lett. **95**, 105502 (2005).
[54] P. E. Blöchl, Phys. Rev. B **50**, 17953 (1994).
[55] B. Hetényi, F. De Angelis, P. Giannozzi, and R. Car, J. Chem. Phys. **115**, 5791 (2001).
[56] G. Henkelman, B. P. Uberuaga, and H. Jónsson, J. Chem. Phys. **113**, 9901 (2000).
[57] G. Henkelman and H. Jónsson, J. Chem. Phys. **113**, 9978 (2000).
[58] J. P. Goss and P. R. Briddon, Phys. Rev. B **75**, 075202 (2007).
[59] H. Yilmaz, B. R. Weiner, and G. Morell, Diamond Relat. Mater. **16**, 840 (2007).

[60] S. J. Breuer and P. R. Briddon, Phys. Rev. B **51**, 6984 (1995).
[61] D. C. Hunt, D. J. Twitchen, M. E. Newton, J. M. Baker, T. R. Anthony, W. F. Banholzer, and S. S. Vagarali, Phys. Rev. B **61**, 3863 (2000).
[62] J. P. Goss, B. J. Coomer, R. Jones, T. D. Shaw, P. R. Briddon, M. Rayson, and S. Öberg, Phys. Rev. B **63**, 195208 (2001).
[63] J. P. Goss, P. R. Briddon, S. Papagiannidis, and R. Jones, Phys. Rev. B **70**, 235208 (2004).
[64] J. P. Goss, P. R. Briddon, and M. J. Shaw, Phys. Rev. B **76**, 075204 (2007).
[65] In the current paper we refer to the split-vacancy structure as *VSV*. Reference 35 which analyzed the structures of a wide range of impurity-vacancy structures both in the split-vacancy form and the simple impurity-vacancy neighboring pair used the alternative notation (S-*V*). However, the analysis in Ref. 35 for (S-*V*) corresponds to the same split-vacancy ground-state geometry analyzed in the current paper.
[66] J. P. Goss, R. Jones, S. J. Breuer, P. R. Briddon, and S. Öberg, Phys. Rev. Lett. **77**, 3041 (1996).
[67] R. Q. Hood, P. R. C. Kent, R. J. Needs, and P. R. Briddon, Phys. Rev. Lett. **91**, 076403 (2003).
[68] J. P. Goss, P. R. Briddon, M. J. Rayson, S. J. Sque, and R. Jones, Phys. Rev. B **73**, 199904(E) (2006).
[69] C. D. Clark, H. Kanda, I. Kiflawi, and G. Sittas, Phys. Rev. B **51**, 16681 (1995).
[70] K. Iakoubovskii and A. Stesmans, Phys. Status Solidi A **186**, 199 (2001).
[71] J. W. Steeds, S. J. Charles, J. Davies, and I. Griffin, Diamond Relat. Mater. **9**, 397 (2000).
[72] R. Farrer, Solid State Commun. **7**, 685 (1969).
[73] R. J. Eyre, J. P. Goss, P. R. Briddon, and J. P. Hagon, J. Phys.: Condens. Matter **17**, 5831 (2005).
[74] M. Katagiri, J. Isoya, S. Koizumi, and H. Kanda, Phys. Status Solidi A **201**, 2451 (2004).